Supporting Material

1. Experiment

1.1 Sample preparation

Samples were prepared using graphene flakes exfoliated from analyzer-grade HOPG and deposited on a doped Si substrate capped with 300nm chlorinated SiO_2. The chlorinated Si/SiO_2 substrates were prepared by Nova Electronics. Hexagonal boron-nitride (h-BN) flakes which are known to reduce the corrugation of graphene were also employed as substrates. Following a transfer procedure similar to that described in (1), we first transfer one layer of graphene on the SiO_2 substrate and then a second graphene layer on top of the first. The metallic leads (Ti/Au) are deposited using standard e-beam lithography. To achieve a clean surface, the sample was baked at 230^oC in forming gas (2).

A necessary requirement to study the effect of charged impurities is to resolve well separated Landau levels (LL) in graphene in the tunneling spectra that are homogeneous over large areas of the sample. We have found that this could be accomplished in graphene samples deposited on graphite or on a second graphene layer (4). In the work reported here we employed a second graphene layer as a buffer between the SiO_2 substrate and the graphene samples studied. The relative angle of rotation between the layers was large, in excess of 10^0. The fact that the twist angle is large ensures decoupling between the layers as evidenced by the observation of spectra characteristic of single layer graphene (5,6). In the samples studied here we obtained sequences of sharp LL characteristic of single layer graphene across large regions. The presence of the second layer doubles the LL degeneracy (4–7) as discussed in the main text.

1.2 Scanning Tunneling Microscopy and Spectroscopy

The experiments were carried out using home-built low temperature (2K-4K) high field (12T-15T) STM and Pt/Ir tips (4,8). The data were taken at temperature T=4.2K. The tunneling conductance dI/dV was measured by lock-in detection with 500 Hz bias voltage modulation. For the spectra presented in this work the voltage modulation was Vm = 5mV. In order to locate micron-sized conductive samples and areas of interest at low temperature on insulating substrates we used the STM tip as a capacitive antenna (9). We then employed LL spectroscopy maps to locate the impurities and characterize their properties.

1.3 Strategy for finding isolated impurities

LL spectroscopy provides an efficient way to identify isolated impurities. The reason is that the LL energy is very sensitive to the local potential (as discussed in the main text), much more so than the typically broad V-shaped spectrum taken in the absence of magnetic field. A typical spectrum taken far from an impurity in the absence of magnetic field is shown in Figure S1(a). Figure S1(b) shows an STM topography image over a large area. The search for impurities starts

by taking LL spectra along a line as show . Figure S1(c) shows an intensity map of these LLs as a function of position along the line. We can clearly see that the energies of the LLs, strongest for N = 0 (for reasons explained in the main text), shift with position reflecting the presence of a potential created by charged impurities. The N = 0 LL moves towards both negative and positive energies suggesting the presence of both positive and negative impurities. We then look for an area that shows a minimal number of impurities such as the one indicated by the arrow in Figure S1(b), where the data in the main text were taken.

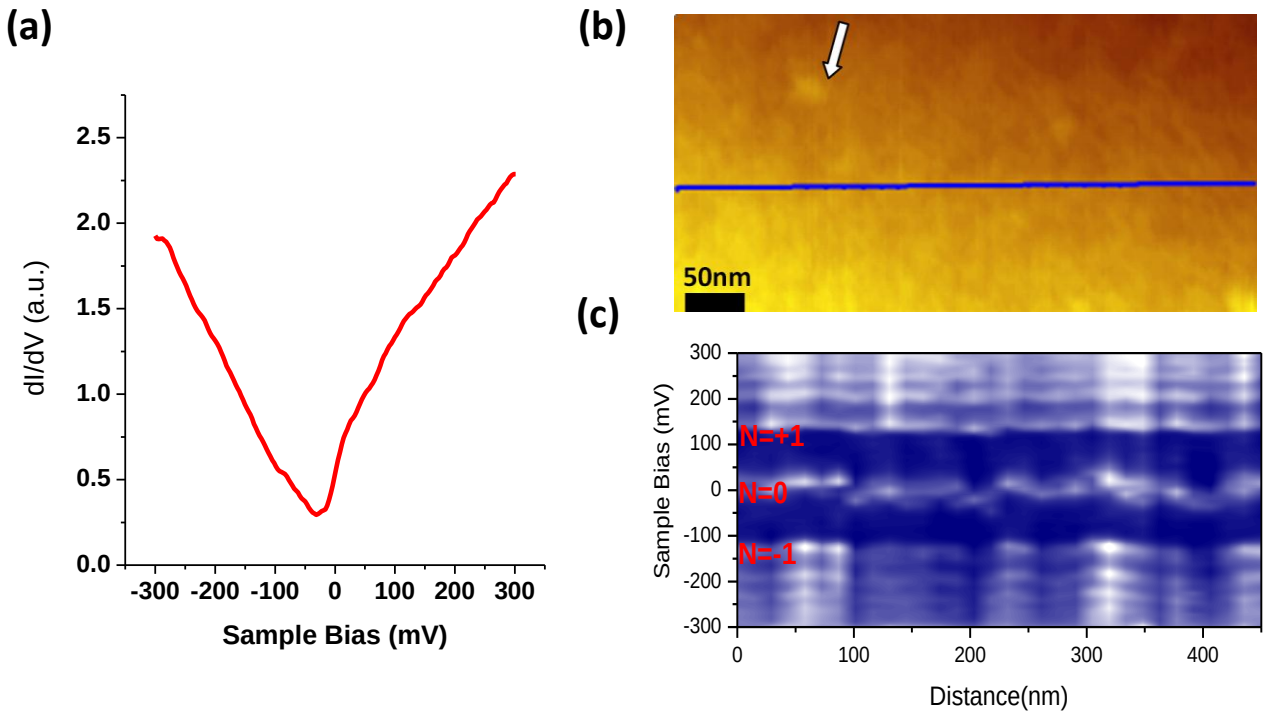

Figure S1: (a) STS away from the impurity in the region where the data in Figure 2(a-c) of the main text were taken. (b) Topographic image indicating the blue line where the spectra in (c) are taken together with the arrow pointing at the region where the impurity in the main text was found. (c) STS line cut along the blue horizontal line in (b); the Landau levels with indices N=0,±1,±2, etc are clearly resolved.

1.4. Regions with overlapping impurity potentials.

As discussed in the main text most of the investigated areas contain impurities that are very close together. An example of such an area was given in Figure 2(d) , (e),(f) of the main text. Although one can clearly observe in the dI/dV maps spectral shifts introduced by the impurities it is not possible to distinguish the contribution from one single impurity in such samples. To further illustrate this point Figure S2(a) shows the topography of that same region as in Figure 2(d) together the line along which the spectra in Figure S2(b) were taken.

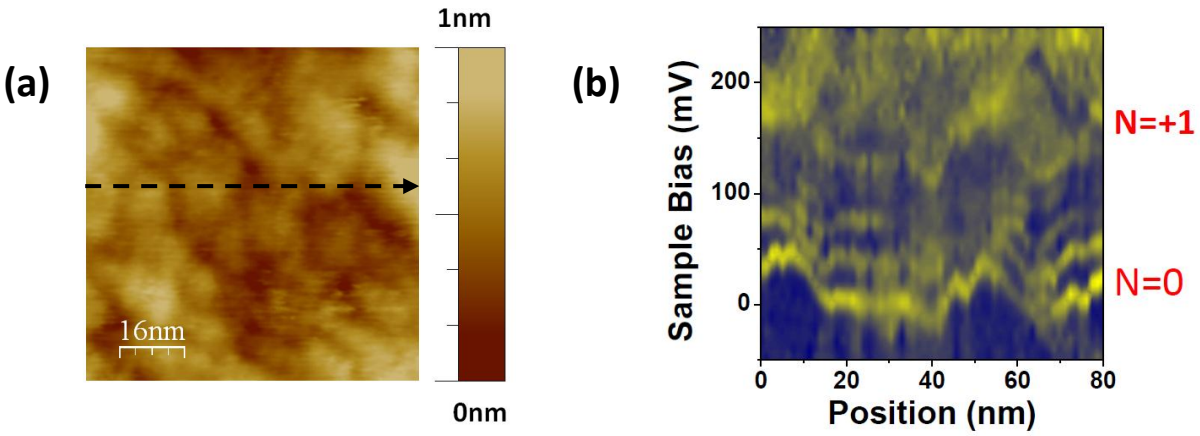

Figure S2: (a) Topography of the area where the data in Figure 2(d-f) of the main text were taken. (b) Spectra taken along the line indicated in (a)

We note that the LL bend around the positions at which charged impurities are located. .However, the fact that the disorder is strong makes it hard to distinguish the sequence of LL specific to single layer graphene and thus to address the question of the effect of a charged impurity.

On samples with less disorder: G+G/SiO_2 we also investigated regions with multiple impurities close together. Figure S3 shows an example of such a region (Figure S3(a)) on the same sample as the data in the main text was taken. The typical spectrum in such a region (Figure S3(b)) shows clear peaks that can be associated with N=0,±1,± etc. The dI/dV maps taken at this region at indicated energies (Figure S3(c)) show the presence of localized states at -30meV and delocalized states at +30meV. To further illustrate how the presence of these impurities affects the LLs, the dI/dV spectra were recorded along three lines that cross the impurities as shown in Figure S3(d). The lines correspond to the ones in Figure S3(a). We observe that consistent with the data in the main text the LL shift near the location of the impurities and if the impurity s strong enough – Line 1- we start to see lifting of the orbital degeneracy of the N=0 LL. All these maps were taken at gate voltage Vg=0V.

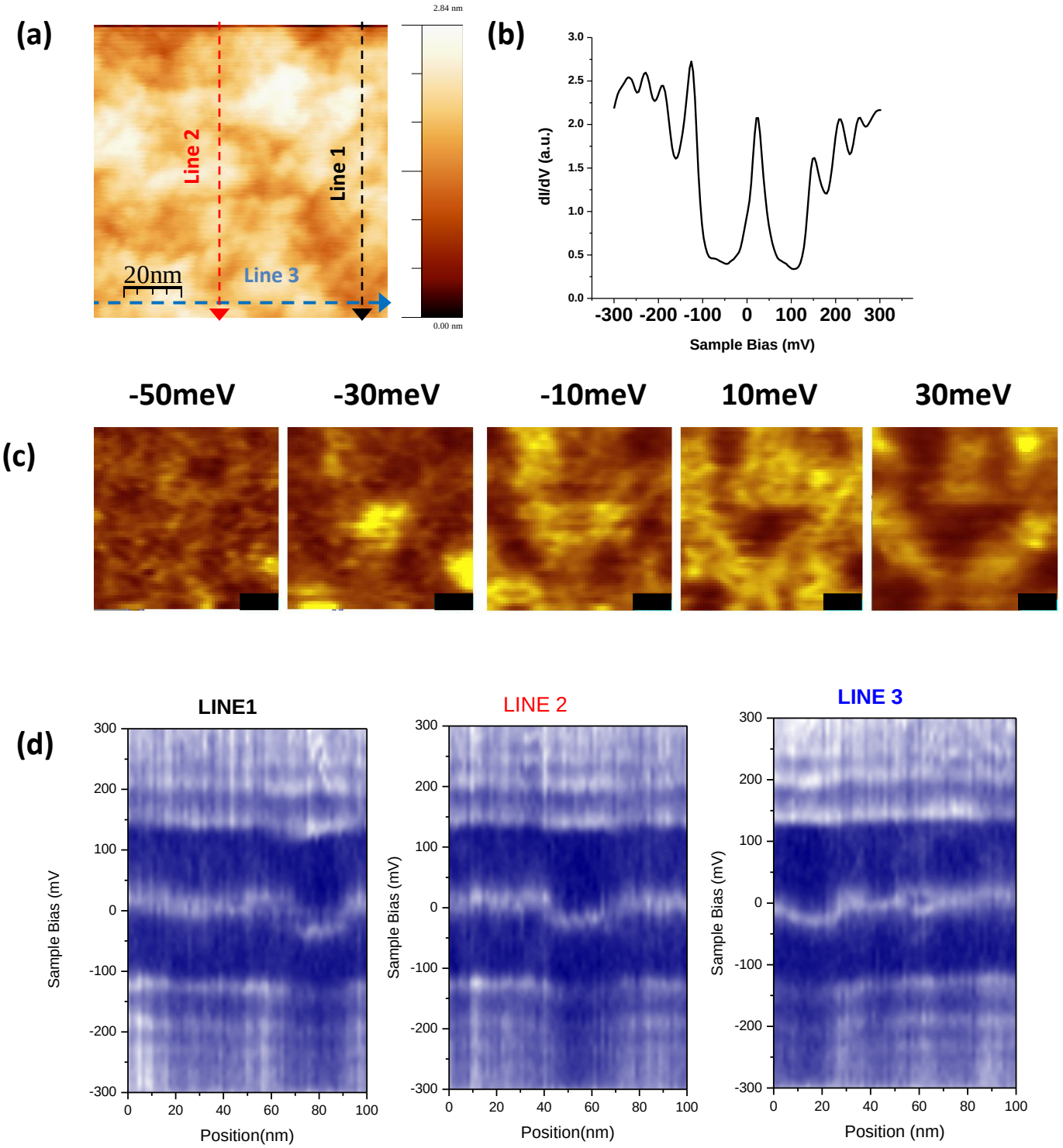

Figure S3 Topography of a region with several close-by impurities. The lines indicate where the data in (d) was taken. (b) STS in a region away from the impurities.
(c) dI/dV maps at sample bias indicated in the top part. The scale bar is 20nm.(d) STS along the lines indicated in (a)

1.5. Effective static dielectric constant of graphene .

To extract the static dielectric constant of bare graphene, κ_{gr} , from the measured value Z/κ we use the relation[10] $\kappa = \kappa_{gr}(\kappa_{(SiO_2)} + 1)/2$. For the SiO_2 substrate, since $\kappa_{(SiO_2)} = 4$, we find $\kappa_{gr}/Z \sim 1$ at V_g=+7V where the N=0 LL is filled. Since according to theory [12,13] graphene provides no screening for full LLs, ie κ_{gr} =1, this implies Z~1. Repeating the procedure for the shifts $E_{00}(V_g)$ at other values of V_g and assuming Z=1 we obtain in Figure S4 the filling dependence of κ_{gr}. We note that screening increases monotonically as filling is reduced, reaching $\kappa_{gr} \approx 5$ for an almost empty LL (V_g=-10V). Comparing this value to the zero field RPA estimate[10] for double layer graphene, $\kappa_{gr} = 1 + g_l g_s g_v \pi r_s/8 \approx 3.3$, shows that screening within a barely filled LL is stronger than in the zero-field case, consistent with the higher DOS available to screening electrons. Here $r_s = \frac{2}{(\kappa_{SiO_2}+1)} \frac{e^2}{4\pi\varepsilon_0\hbar v_F}$ measures the relative strength of the potential and kinetic energies in an interacting quantum Coulomb system. The absence of screening for filled states indicates that strong interactions should be present when the Fermi level lies in a gap, consistent with the observation of a fractional QHE in suspended graphene [14,15]. We note that in zero-filed, where Z/κ~0.1, the impurity is subcritical and that the magnetic-field is crucial for accessing the supercritical regime.

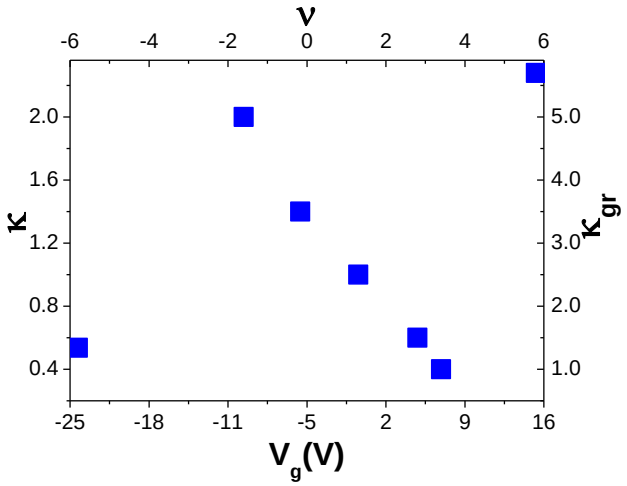

Figure S4. Filling dependence of the dielectric constant of graphene. Screening decreases monotonically with filling reaching its lowest value for full LLs.

2 Theory: Wave functions in graphene in a magnetic field

Here we present the eigenfunctions in graphene in the magnetic field. The Dirac Hamiltonian in Equation (2) has the following form

$$H_0 = v_F \begin{pmatrix} 0 & \hat{p}_- - eA_- \\ \hat{p}_+ - eA_+ & 0 \end{pmatrix}$$

in the AB sublattice space, where $\hat{p}_\pm = \hat{p}_x \pm \mathrm{i}\hat{p}_y$, $A_\pm = A_x \pm \mathrm{i}A_y$, $\hat{p}_{x,y} = \mathrm{i}\hbar\partial_{x,y}$ are the components of the momentum operator and $\mathbf{A} = (A_x, A_y, 0)$ is the vector potential due to the magnetic field $\mathbf{B} = (0, 0, B)$. In the symmetric gauge $\mathbf{A} = \frac{1}{2}[\mathbf{B} \times \mathbf{r}] = \frac{1}{2}B(-y, x, 0)$, convenient for dealing with radially symmetric potentials, the eigenfunctions of the Hamiltonian $\hat{H}_0$ can be sought in the form

$$\psi = \frac{1}{\sqrt{2\pi}} \begin{pmatrix} \mathrm{e}^{\mathrm{i}m\varphi} R_A(r) \\ \mathrm{e}^{\mathrm{i}(m+1)\varphi} R_B(r) \end{pmatrix},$$

where m is an integer angular momentum quantum number and (r, φ) are the polar coordinates, $x = r\cos\varphi$, $y = r\sin\varphi$. Substituting this form into the equation

$$\hat{H}_0\psi = E\psi$$

yields the system of equations

$$-\mathrm{i}\hbar v_F \left(\partial_r + \frac{m+1}{r} - \frac{r}{2l_B^2}\right) R_B(r) = E R_A(r), \; -\mathrm{i}\hbar v_F \left(\partial_r - \frac{m}{r} + \frac{r}{2l_B^2}\right) R_A(r) = E R_B(r), \tag{1}$$

for the radial functions $R_{A,B}(r)$. One can obtain the second-order equations

$$\left[\partial_r^2 + \frac{1}{r}\partial_r - \frac{m^2}{r^2} - \left(\frac{r}{2l_B^2}\right)^2 + \frac{m+1}{l_B^2} + \left(\frac{E}{\hbar v_F}\right)^2\right] R_A(r) = 0, \tag{2}$$

$$\left[\partial_r^2 + \frac{1}{r}\partial_r - \frac{(m+1)^2}{r^2} - \left(\frac{r}{2l_B^2}\right)^2 + \frac{m}{l_B^2} + \left(\frac{E}{\hbar v_F}\right)^2\right] R_B(r) = 0 \tag{3}$$

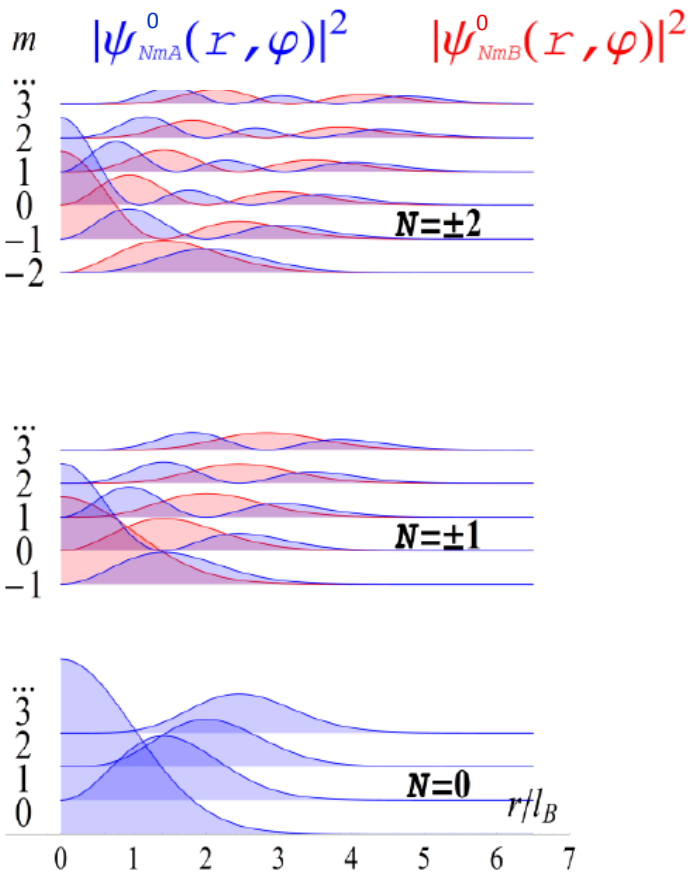

Figure S5. Calculated probability densities, $\left|\psi^0_{NmA}(r,\varphi)\right|^2$ and $\left|\psi^0_{NmB}(r,\varphi)\right|^2$, on A (blue) and B (red) sublattices of graphene in a magnetic field.

References

1. C. Dean, et al., Nature nanotechnology 5, 722 (2010).

2. A. Luican, G. Li, E. Y. Andrei, Phys. Rev. B 83, 041405 (2011).

3. S. Jung et al., Nat. Phys. 7, 245 (2011)

4. G. Li, A. Luican, E. Y. Andrei, Phys. Rev. Lett. 102, 176804 (2009).

5. A. Luican, et al., Phys. Rev. Lett. 106, 126802 (2011).

6. J. D. Sanchez-Yamagishi, et al., Phys. Rev. Lett. 108, 076601 (2012).

7. D. S. Lee, et al., Phys. Rev. Lett. 107, 216602 (2011).

8. G. Li, E. Andrei, Nature Physics 3, 623 (2007).

9. G. Li, A. Luican, E. Y. Andrei, Review of Scientific Instruments 82, 073701 (2011).

10. Hwang, E. H. & Das Sarma, S. Dielectric function, screening, and plasmons in two-dimensional graphene. Physical Review B 75, 205418 (2007).

11. Hwang, E. H. & Das Sarma, S. Dielectric function, screening, and plasmons in two-dimensional graphene. Physical Review B 75, 205418 (2007).

12. Xie, X. C., Li, Q. P. & Das Sarma, S. Density of states and thermodynamic properties of a two-dimensional electron gas in a strong external magnetic field. Physical Review B 42, 7132-7147 (1990).

13. Pyatkovskiy, P. K. & Gusynin, V. P. Dynamical polarization of graphene in a magnetic field. Physical Review B 83, 075422 (2011).

14. Du, X., Skachko, I., Duerr, F., Luican, A. & Andrei, E. Y. Fractional quantum Hall effect and insulating phase of Dirac electrons in graphene. Nature 462, 192 (2009).

15. Bolotin, K. I., Ghahari, F., Shulman, M. D., Stormer, H. L. & Kim, P. Observation of the fractional quantum Hall effect in graphene. Nature 462, 196-199 (2009).